THE JOURNAL OF PHYSICAL CHEMISTRY B

Article

pubs.acs.org/JPCB

Assembly of Oppositely Charged Microgels at the Air/Water Interface

Daisuke Suzuki* and Koji Horigome

Graduate School of Textile Science and Technology, Shinshu University, 3-15-1, Tokida, Ueda 386-8567, Japan

Supporting Information

ABSTRACT: We present an assembly of cationic and anionic microgels at the air/water interface. Monodispersed, micrometer-sized, and oppositely charged microgels were synthesized by aqueous free-radical precipitation polymerization by using *N*-isopropylmethacrylamide, comonomers, and cross-linkers. The oppositely charged microgels were prepared by using different types of water-soluble initiators. These microgels were mixed in a solution to assemble them at the air/water interface. In particular, linear and branched chainlike structures of the microgels were spontaneously formed at the air/water interface. Effects of salt concentration, microgel concentration, and number ratio of cationic and anionic microgels on the structures of microgel assembly were investigated by optical microscopy and scanning electron microscopy.

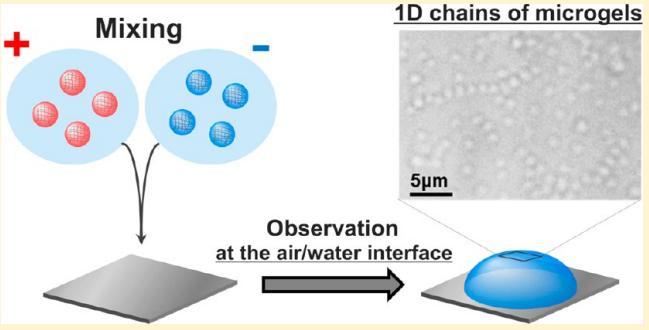

INTRODUCTION

The assembly of nano-/micrometer particles has been of considerable interest due to the unique optical, electrical, and magnetic properties that lead to promising applications such as data storage, sensors, and photonic crystals.[1−3] These particles have been assembled into one-dimensional (1D) chains, two-dimensional (2D) films, three-dimensional (3D) crystals, and complex colloidal aggregates. In the case of 1D chains, the structures are of special interest since they show unique functions such as the directional transfer of photons, electrons, and spins.[4] So far, the 1D structures can be fabricated by using linear templates such as polyelectrolytes, biomolecules, inorganic nanowires, and lithographic patterns.[5−9] Furthermore, the 1D structures can be constructed by applying external electric/magnetic fields.[10−13] Different from 2D or 3D assemblies, the formation of 1D assembly is difficult by using isotropic particles solely. Anisotropic particles called Janus particles can be assembled into 1D structures.[14−17] For example, particle chains were formed from dipolar particles produced by micro contact printing techniques.[14] Anisotropic hairy particles were assembled into chainlike structure with each other through Au and thiol group reaction.[15] However, the precise control of 1D assembly of particles in a solution is still challenging research because of the difficulty in controlling colloidal interactions such as van der Waals force and electrostatic force.

Hydrogel particles (microgels) are spherical, cross-linked polymeric networks swollen by a good solvent. Compared to hard particles, soft microgels have possibilities to exhibit unique colloidal behavior that has never been observed before using hard particles. Microgels have attracted much attention due to their stimuli-responsive properties: physical/chemical properties of microgels change in response to external stimuli such as temperature, pH, light, chemical reaction.[18−26] Therefore, many applications such as drug delivery systems, chemical/biological separation, actuators, photonic crystals, smart emulsifiers, microreactors, and sensors have been proposed by using microgels.[27−46] In addition, microgels show soft repulsive interactions arising from the repulsion between hydrated polymer chains located at the exterior of microgels. We assume if attractive/repulsive interactions between microgels were controlled precisely, complex structures of particles such as 1D chains can be formed by just mixing solutions.

In this paper, we present the results of our research on 1D chains of microgels formed spontaneously in a solution. To achieve this goal, cationic and anionic microgels were synthesized by precipitation polymerization by using methacrylamide derivative, comonomers, and cross-linkers. To produce oppositely charged microgels, different types of water-soluble initiators were used for the polymerization. These microgels were mixed in a solution to assemble them into 1D chains at the air/water interface. Effects of salt concentration, microgel concentration, and number ratio of cationic and anionic microgels on the structures of microgel assembly were investigated by optical microscopy and scanning electron microscopy. In addition, the mechanism of 1D chains formation by mixing oppositely charged microgels will also be discussed.

Received: April 9, 2013
Revised: June 13, 2013

dx.doi.org/10.1021/jp4035166 | J. Phys. Chem. B XXXX, XXX, XXX−XXX

EXPERIMENTAL DETAILS

Materials. *N*-Isopropylmethacrylamide (NIPMAm, 97%) and *N*,*N*′-(1,2-dihydroxyethylene)bisacrylamide (DHEA, 97%) were purchased from Sigma-Aldrich Co. LLC. *N*,*N*′-Methylenebis(acrylamide) (BIS, 97%), 3-(methacryloylamino)-propyltrimethylammonium chloride (MAPTAC, 96%), acrylic acid (AAc, 98%), 2,2′-azobis(2-methylpropionamidine) dihydrochloride (V-50, 95%), potassium peroxodisulfate (KPS, 95%) and sodium chloride (NaCl, 99.5%) were purchased from Wako Pure Chemical Industries, Ltd.. All reagents were used as received. Polystyrene (PS) substrate (Iwaki, 60 mm/Non-treated Dish, Asahi Glass Co., Ltd.) was used as received. Water for all reactions, solution preparation, and polymer purification was first distilled then ion-exchanged (EYELA, SA-2100E1).

Preparation of Cationic Microgels. Positively charged microgels were prepared by aqueous free-radical precipitation polymerization by using the cationic initiator 2,2′-azobis(2-methylpropionamidine) dihydrochloride (V-50). A small amount of the cationic monomer 3-(methacryloylamino)-propyltrimethylammonium chloride (MAPTAC) was copolymerized to adjust the electrostatic property since positive charges from V-50 residues were not enough to show positive values of electrophoretic mobility. A mixture of *N*-isopropylmethacrylamide (NIPMAm; 0.896 g, 94 mol %), *N*,*N*′-methylenebis(acrylamide) (BIS; 0.058 g, 5 mol %), MAPTAC (0.0176 g, 1 mol %), and water (45 mL) was poured into a 50 mL three-neck, round-bottom flask equipped with a mechanical stirrer, a condenser, and nitrogen gas inlet. The initial total monomer concentration was held constant at 150 mM. Herein, NaCl was added to the solution to suppress the Coulomb repulsion arising from MAPTAC during the polymerization and to adjust the obtained microgel size (total concentration 10 mM). The monomer solution was bubbled for 30 min with nitrogen gas to purge oxygen at 70 °C. Under a stream of nitrogen and with constant stirring at 250 rpm, the initiator V-50 (0.027 g) dissolved in 5 mL of water was injected into the flask to start the polymerization. Then the polymerization continued for 4 h. After the polymerization, the microgel dispersion was cooled to room temperature. The microgels were purified by centrifugation/redispersion with water twice using a relative centrifugal force (RCF) of 20000*g*, and by means of dialysis. The microgels were denoted as N(+). The chemical structure of the microgel is shown in Figure 1.

Preparation of Anionic Microgels. The method to produce negatively charged microgels was almost the same as that for positively charged microgels mentioned above. Negatively charged microgels were prepared by aqueous free-radical precipitation polymerization by using the anionic initiator potassium peroxodisulfate (KPS). A mixture of NIPMAm (1.812 g, 95 mol %), BIS (0.115 g, 5 mol %), and water (95 mL) was poured into a 300 mL three-neck, round-bottom flask equipped with a mechanical stirrer, a condenser, and nitrogen gas inlet. The initial total monomer concentration was fixed at 150 mM. The monomer solution was bubbled for 30 min with nitrogen gas to purge oxygen at 70 °C. Under a stream of nitrogen and with constant stirring at 250 rpm, the initiator KPS (0.053 g) dissolved in 5 mL of water was injected to the flask to start the polymerization. Then the polymerization continued for 4 h. After the polymerization, the microgel dispersion was cooled to room temperature. The microgels were purified by centrifugation/redispersion with water twice using a RCF of 20000*g*, and by means of dialysis.

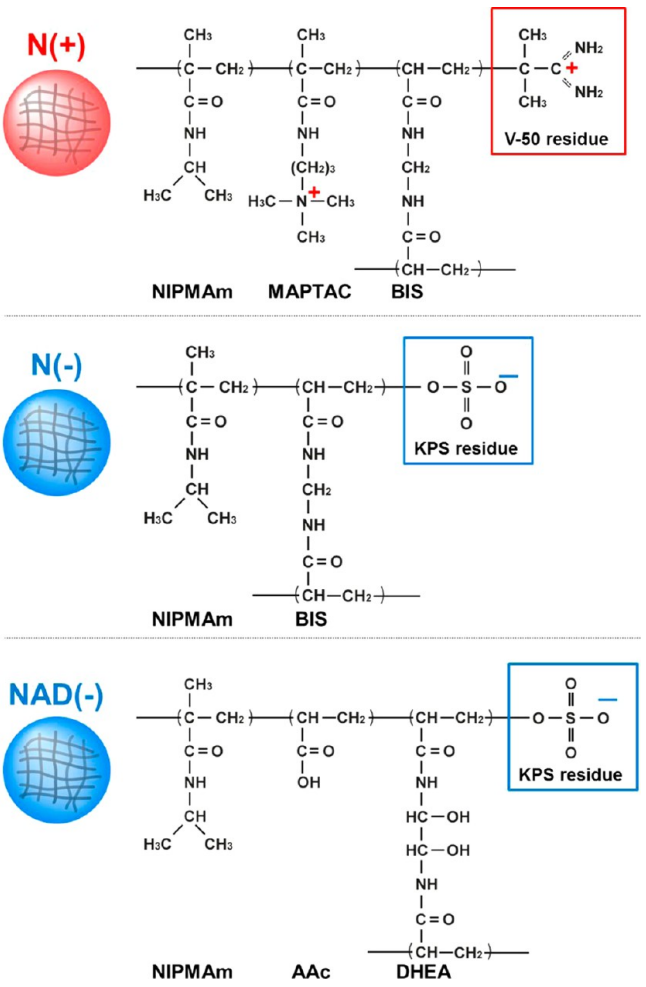

Figure 1. Schematic illustration of chemical structures of the microgels in this study.

The microgels were denoted as N(−). The chemical structure of the microgel is shown in Figure 1.

Preparation of Anionic, Degradable Microgels. To investigate the structure of microgel assemblies, negatively charged degradable microgels were synthesized by aqueous free radical precipitation polymerization by using degradable cross-linker.[47] A mixture of NIPMAm (0.572 g, 60 mol %), acrylic acid (AAc; 0.162 g, 30 mol %), *N*,*N*′-(1,2-dihydroxyethylene)-bisacrylamide (DHEA; 0.15 g, 10 mol %), and water (45 mL) was poured into a 200 mL three-neck, round-bottom flask equipped with a mechanical stirrer, a condenser, and nitrogen gas inlet. The initial total monomer concentration was fixed at 150 mM. The monomer solution was bubbled for 30 min with nitrogen gas to purge oxygen at 70 °C. Under a stream of nitrogen and with constant stirring at 250 rpm, the initiator KPS (0.015 g) dissolved in 5 mL of water was injected to the flask to start the polymerization. Then the polymerization continued for 4 h. After the polymerization, the microgel dispersion was cooled to room temperature. The microgels were purified by centrifugation/redispersion with water twice using a RCF of 20000*g*. The microgels were denoted as NAD(−). The chemical structure of the microgel is shown in Figure 1.

Characterization of Microgels. The hydrodynamic diameters of each microgel were characterized by dynamic light scattering (DLS; Malvern Instruments Ltd., ZetasizerNa-

dx.doi.org/10.1021/jp4035166 | J. Phys. Chem. B XXXX, XXX, XXX−XXX

Table 1. Chemical Composition, Hydrodynamic Diameter (D_h), and Electrophoretic Mobility (EPM) of the Microgels

					D_h (nm)		EPM[a] (10^{-8} m^2 V^{-1} s^{-1})	
code	NIPMAm (mol %)	cross-linker (mol %)	comonomer (mol %)	initiator	25 °C	60 °C	25 °C	60 °C
N(+)	94	BIS 5	MAPTAC 1	V-50	1380	520	0.54	2.7
N(−)	95	BIS 5	−	KPS	1500	500	−0.49	−3.6
NAD(−)	60	DHEA 10	AAc 30	KPS	1350	720	−1.60	−3.0

[a]Measured in a 1 mM NaCl solution.

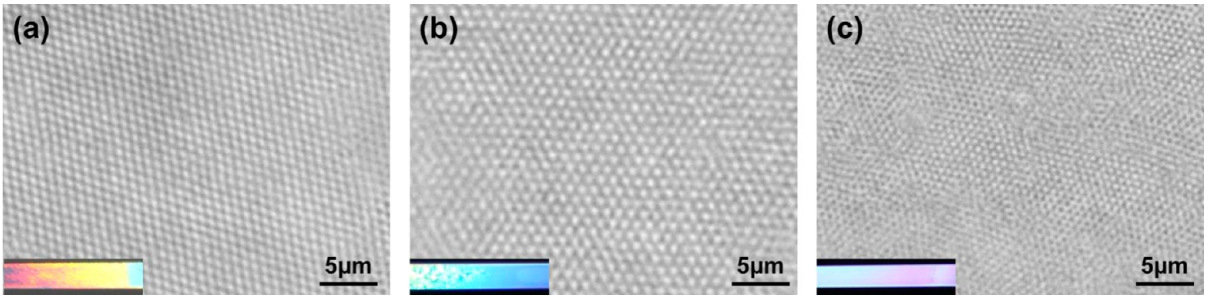

Figure 2. Optical microscope images of microgel colloidal crystals assembled from (a) N(+), (b) N(−), and (c) NAD(−) microgels in deionized water at 25 °C. Microgel concentrations are 5.0 wt % in all cases. Insets are photographs of each microgel assembly in the rectangular capillary tubes.

noS). DLS data were an average of 15 measurements with 30 s acquisition times. The microgels were analyzed at a concentration of ∼0.005 wt %. NaCl was then used to adjust to 1 mM total salt concentration. The samples were allowed to equilibrate thermally at the desired temperature for 10 min before the measurements. Scattered light was collected at 173°. The hydrodynamic diameters of the microgels were determined from the measured diffusion coefficients by using the Stokes−Einstein equation (Zetasizer software v6.12).

The electrophoretic mobilities (EPM) of microgels were measured with a ZetasizerNanoZS (Malvern, Zetasizer software Ver. 4.20). The EPM data were an average of three measurements. The samples were allowed to equilibrate thermally at the desired temperature for 10 min before the measurements. The microgels were analyzed at a concentration of ∼0.005 wt %. NaCl was used to adjust salt concentration.

The microgels in an aqueous solution were observed with an optical microscope (BX51, Olympus) equipped with a digital camera (ImageX Earth Type S-2.0 M Ver.3.0.5, Kikuchi-Optical Co., Ltd.). The microgels were transferred into Vitrotube borosilicate rectangular capillaries (0.1 × 2.0 mm) by capillary action. Herein, in order to observe the microgel clearly, colloidal crystals of the microgels were formed through the thermal annealing process.[33,34]

The microgels dried on the polystyrene substrate were observed by scanning electron microscopy (SEM, Hitachi Ltd., S-3000N). The samples were sputtered with Pt/Pd before the observation.

Observation of the Microgel Assembly. The cationic and the anionic microgel dispersions were mixed and put on the polystyrene substrate and dried at room temperature (25 ± 2 °C, humidity <20%). The total volume of the mixtures was 20 μL. Then, the interfaces of the air/water and the solid/water and droplets of the microgel dispersions were observed with the optical microscope as a function of time. Influences of the salt concentration, microgel concentration, and number ratio of the cationic and anionic microgels on the assembly were investigated.

RESULTS AND DISCUSSION

Synthesis and Characterization of Microgels. The synthesis of the microgels was carried out by aqueous free-radical precipitation polymerization. This is a conventional method for preparing temperature-responsive microgels, as the monomer is soluble under the reaction conditions, but the polymer undergoes a phase separation into globules.[18] In this study, we chose poly(*N*-isopropylmethacrylamide) (pNIPMAm) as a polymer for the mainframe of the microgels. pNIPMAm is extensively studied temperature-responsive polymer, which exhibits a lower critical solution temperature (LCST) around ∼44 °C in aqueous media.[48−50] Thus, the microgels composed of the polymers show a volume phase transition temperature (VPTT) around the LCST. In this case, to observe microgel assemblies, micrometer-sized, large microgels were synthesized. Table 1 summarizes the chemical composition, hydrodynamic diameters (D_h), and electrophoretic mobility (EPM) of the microgels used in this study. Basically, N(+) and N(−) microgels were used for a series of the studies. The D_h of these microgels were both ∼1.5 μm in their swollen states, and EPM indicates that they are positively and negatively charged microgels, respectively. In addition, EPM increased with a rise in temperature due to the decrease in their volume and increment of charge density of microgel surfaces.[51] For NAD(−) microgels, EPM showed higher value at the swollen state than that of N(−) microgels. This is because of the incorporation of the charged comonomer, acrylic acid, into NAD(−) microgels. In this study, assembly of the microgels was investigated by using the swollen microgels at 25 °C.

In order to check the monodispersity of these microgels, colloidal crystals of these microgels were formed and visualized by optical microscopy. The colloidal crystals were formed as follows: first, concentrated and viscous microgel dispersions (5 wt %) were heated above the VPTT to obtain low-viscosity dispersions due to the expulsion of water from the microgels. Then rectangular glass tubes were loaded by capillary action by inserting each tube into the heated dispersions. After the tube ends were sealed to prevent evaporation, the tubes were slowly cooled to 25 °C. Figure 2 shows representative optical

dx.doi.org/10.1021/jp4035166 | J. Phys. Chem. B XXXX, XXX, XXX−XXX

microscope images for these microgels together with photographs of each sample within the capillary tubes. From these images, it is confirmed that the microgels are large enough to be traced by the optical microscopy. These images demonstrate that the microgels are ordered hexagonally and in close contact with one another, resulting in structural color. The ordered structure of the microgels indicates that the microgels are monodispersed. The sizes of the microgels in the capillary tubes were estimated 0.9 μm for N(+), 1.0 μm for N(−), and 0.8 μm for NAD(−) microgels at 25 °C.

Figure 3 shows EPM values of N(+) and N(−) microgels as a function of NaCl concentration at 25 °C, where the microgels

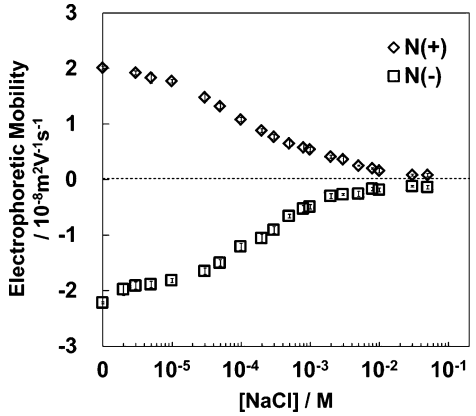

Figure 3. Electrophoretic mobility for N(+) (open diamonds) and N(−) microgels (open squares) measured at 25 °C as a function of NaCl concentration.

are in the swollen states. It is generally known that EPM values are relatively low when the microgels are in the swollen states, but the values increase due to the increased charge density by expelling a large amount of water molecules from microgels.[51] Herein, we found that the EPM value is dependent on salt concentration when the microgels are in the swollen states: the changes in EPM are attributed to the charge screening effect of electrolyte. At high NaCl concentrations (>10 mM), EPM was almost zero for both N(+) and N(−) microgels. However, there are large differences of EPM between N(+) and N(−) microgels at low NaCl concentrations, especially when no NaCl was added. In addition, because of the steric repulsive interaction between microgels, we considered that these oppositely charges microgels can be attracted by electrostatic force much slower than hard particles such as polystyrene and silica particles.

Assembly of Oppositely Charged Microgels at the Air/Water Interface. First, N(+) and N(−) microgels were simply mixed and observed with a digital camera in order to check the colloidal stability of the binary mixture of N(+) and N(−) microgels. Figure 4 shows photographs of the binary mixtures of N(+) and N(−) microgels at 25 °C. Herein, NaCl concentration is different in each sample. When NaCl concentration was low (0−0.1 mM, Figure 4a−c), these microgels were flocculated rapidly just after the mixing, and the dispersions became transparent. With increasing NaCl concentration (0.3 and 0.5 mM), the mixtures gradually settled down, indicating these microgels were slowly flocculated under these conditions. Finally, flocculation was not observed when NaCl concentration was higher than 3 mM (Figure 4f−j). Note that the binary mixtures of N(+) and N(−) microgels showed

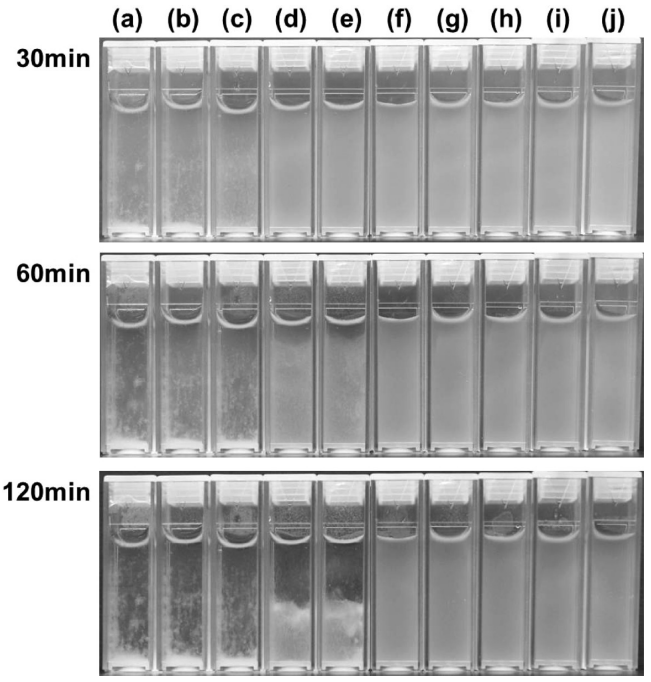

Figure 4. Photographs of the binary mixtures of N(+) and N(−) microgels at 25 °C as a function of NaCl concentration: (a) 0, (b) 1 × 10^{-5}, (c) 1 × 10^{-4}, (d) 3 × 10^{-4}, (e) 5 × 10^{-4}, (f) 3 × 10^{-3}, (g) 5 × 10^{-3}, (h) 1 × 10^{-2}, (i) 1 × 10^{-1}, and (j) 1 M. Total microgel concentration was 0.05 wt % in each case.

fast flocculation irrespective of NaCl concentration above the VPTT of these microgels.[52] On the other hand, colloidal stability of the mixtures could be tuned by NaCl concentration below the VPTT (see Figure S1 in the Supporting Information). Therefore, salt concentration dependence on colloidal stability of the binary mixtures of N(+) and N(−) microgels shown in Figure 4 can be interpreted as follows: At low NaCl concentrations, these microgels were flocculated rapidly due to strong electrostatic attractive force between the microgels. With increasing NaCl concentration, surface charges of the microgels were screened and the electrostatic attractive force became weaker. Thus, the rate of flocculation was slower, and finally the mixture did not show flocculation at higher NaCl concentrations. Dependence of NaCl concentration on EPM shown in Figure 3 well supports the phenomenon. The salt-dependent colloidal behavior of the binary mixture of oppositely charged microgels is unique. Recently, this type of the behavior has been reported in several papers.[52−54] For example, Spruijt et al. used the polystyrene particles synthesized by dispersion polymerization using poly(vinylpyrrolidone) as a stabilizer, and then positively or negatively charged polyelectrolyte brushes were grafted from the surfaces of the particle using aqueous atom transfer radical polymerization. Russell et al. used colloidal particles polymerized from *tert*-butyl methacrylate and trifluoroethyl methacrylate, and positively or negatively charged polyelectrolyte brushes were polymerized from initiators incorporated on the particle surface. Different from our case, these previous works did not use the air/water interface for particle assemblies. When the microgels are in the swollen state, the interparticle van der Waals attraction become negligible because the polymer volume fraction (Φ_p) is very small.[55] The analytical equation for the van der Waals attraction of microgels, $G_A(h)$, between two identical spherical particles of

dx.doi.org/10.1021/jp4035166 | J. Phys. Chem. B XXXX, XXX, XXX−XXX

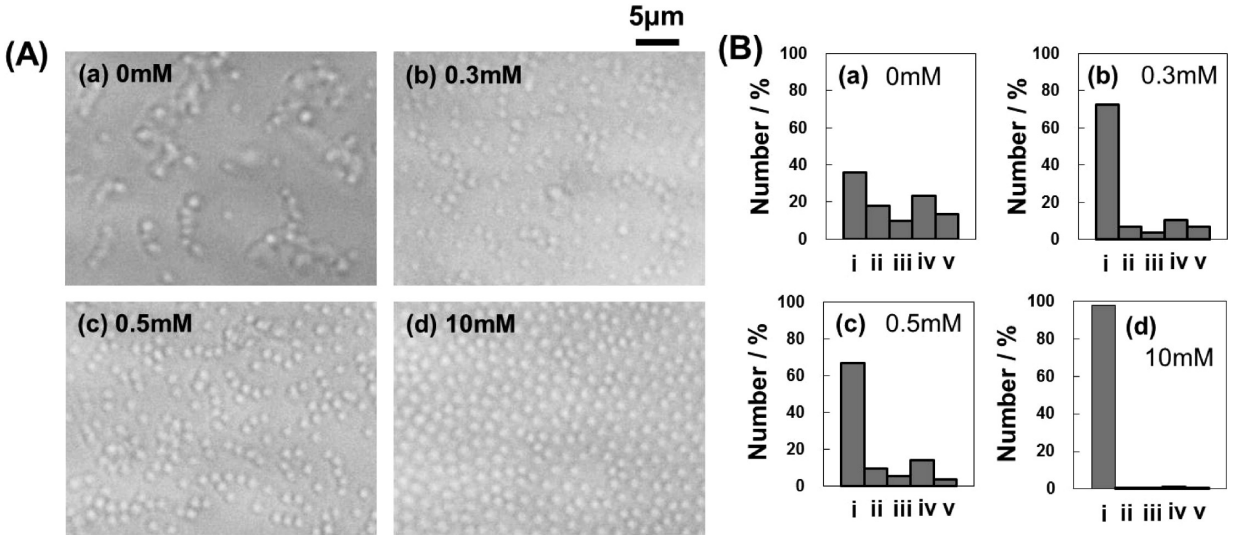

Figure 5. (A) Optical microscope images of the binary mixtures of N(+) and N(−) microgels at 25 °C as a function of NaCl concentration; (a) 0, (b) 0.3, (c) 0.5, and (d) 10 mM. Total microgel concentration was 0.0025 wt % in each case. The air/water interfaces were observed in all cases due to the adsorption of these microgels; see Figure S2. The images were taken after 50 min of the mixing. (B) Number distribution of microgels and microgel assemblies for the binary mixtures of N(+) and N(−) microgels shown in (A): (i) monomer, (ii) dimer, (iii) trimer, (iv) chainlike assembly (more than four microgels), and (v) aggregates. Microgels or microgel assemblies observed per unit area (3640 μm^2) were counted.

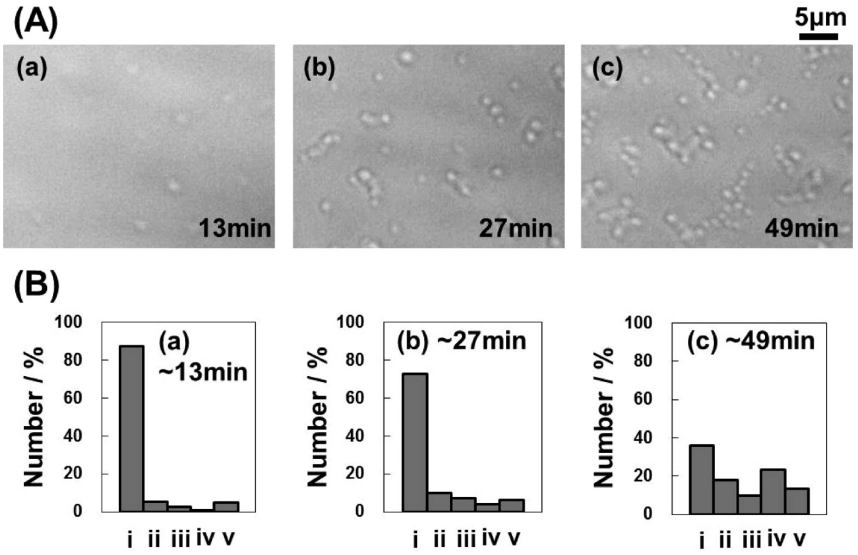

Figure 6. (A) Optical microscope observation of the binary mixtures of N(+) and N(−) microgels at 25 °C as a function of time; The images were taken (a) 13, (b) 27, and (c) 49 min after the mixing. No NaCl was added. Total microgel concentration was 0.0025 wt % in each case. The air/water interfaces were observed in all cases. Concentration ratio of N(+) and N(−) microgels was 1:1 (wt %/wt %). (B) Number distribution of microgels and microgel assemblies for the binary mixtures of N(+) and N(−) microgels shown in (A): (i) monomer, (ii) dimer, (iii) trimer, (iv) chainlike assembly (more than four microgels), and (v) aggregates. Microgels or microgel assemblies observed per unit area (3640 μm^2) were counted.

radius a as a function of surface to surface, h, Hamaker constant of the solvent, A_s, and that of the polymer, A_p, is that given by Vincent as follows.[55]

$$G_A = -(A_p^{1/2} - A_s^{1/2})^2 \Phi_p^2 a/12h$$

Thus, the unique behavior shown in Figure 4 must be due to soft repulsive interactions arising from the repulsion between hydrated polymer chains located at the exterior of microgels.

Next, these binary mixtures of N(+) and N(−) microgels were observed directly by optical microscopy. For the observation, each dispersion was mixed with a pipet on a polystyrene substrate. Total microgel concentration was fixed at 0.0025 wt %; microgel chains could not be distinguished at higher microgel concentrations (see Figure S2 in the Supporting Information). Herein, almost all microgels were adsorbed at the air/water interfaces within a few minutes (see Figure S3 in the Supporting Information). This adsorption may be related to amphiphilic property of NIPMAm monomer and its polymer: a similar acrylamide derivative, *N*-isopropylacrylamide (NIPAm),[56,57] shows surface activity irrespective of polymer and microgels,[58,59] and they adsorb at the air/water interface.[60] Therefore, we observed microgels and microgel assemblies at the air/water interface in this study. Figure 5A shows representative images of microgels and microgel

dx.doi.org/10.1021/jp4035166 | J. Phys. Chem. B XXXX, XXX, XXX−XXX

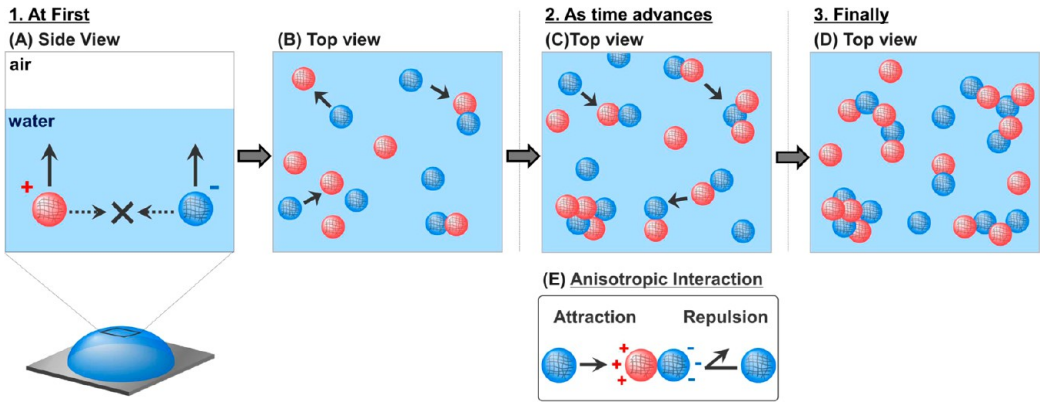

Figure 7. Schematic illustration of the mechanism of assembly of oppositely charged microgels at the air/water interface. (A) Cationic and anionic microgels are adsorbed mainly near the air/water interface, respectively. (B) The microgels assembled with each other by electrostatic interaction. (C) The microgels, dimer, and trimer are formed with each other; see movies in the Supporting Information. (D) Linear and branched chains of microgels are formed. (E) Example of anisotropic interaction.

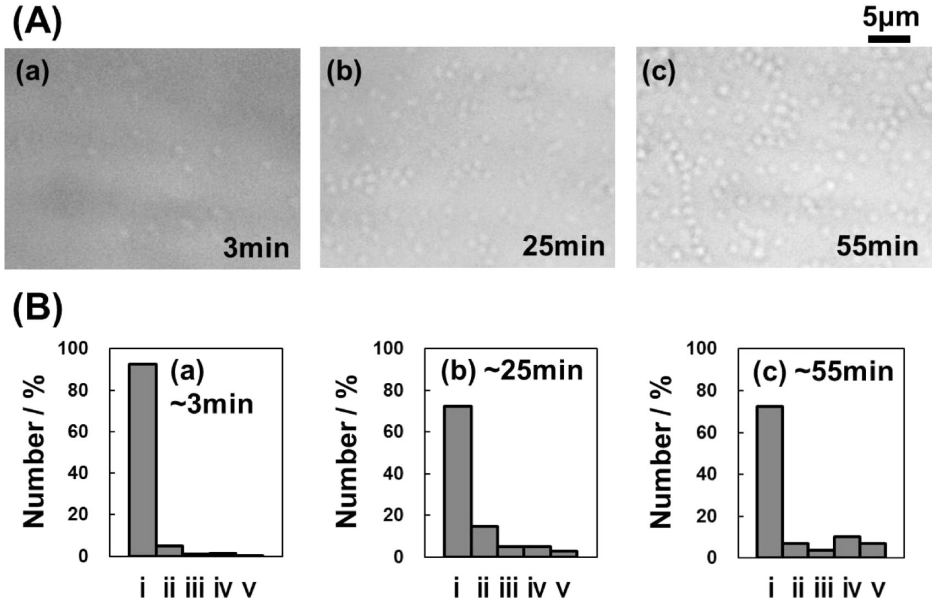

Figure 8. (A) Optical microscope observation of the binary mixtures of N(+) and N(−) microgels at 25 °C as a function of time. The images were taken (a) 3, (b) 25, and (c) 55 min after the mixing. NaCl concentration was 0.3 mM. Total microgel concentration was 0.0025 wt % in each case. The air/water interfaces were observed in all cases. Concentration ratio of N(+) and N(−) microgels was 1:1 (wt %/wt %). (B) Number distribution of microgels and microgel assemblies for the binary mixtures of N(+) and N(−) microgels shown in (A): (i) monomer, (ii) dimer, (iii) trimer, (iv) chain like assembly (more than four microgels), and (v) aggregates. Microgels or microgel assemblies observed per unit area (3640 μm^2) were counted.

assemblies at the air/water interface. These images were taken after 50 min from the mixing because the spatial distribution of microgels at the air/water interface did not change so much after 50 min. Figure 5B summarizes the structures of microgels as follows: (i) monomer (single microgel), (ii) dimer, (iii) trimer, (iv) chainlike assembly (more than four microgels), and (v) random aggregates. As can be seen from Figure 5A, microgel chains were formed at low NaCl concentrations (0, 0.3, and 0.5 mM). However, microgel chains and other assemblies were not formed when the NaCl concentration was higher (10 mM), and hexagonally ordered structure was observed (Figure 5A(d)). The ordered structure of microgels at the air/water interface had already been observed before when pNIPAm microgel dispersions were observed by optical microscopy.[60] In this study, electrostatic attractive force between N(+) and N(−) microgels was suppressed by the presence of 10 mM NaCl, and similar structure to sole pNIPAm microgels was observed at the air/water interface. With decreasing NaCl concentration, electrostatic attractive force between N(+) and N(−) microgels was stronger, and these microgels were assembled with each other near the air/water interface, and linear and branched chains were observed. In particular, there is a difference between with and without NaCl as shown in Figure 5B(a−c). Here, the length of the linear and branched chains was measured with ImageJ (Ver. 1.45s), and summarized in Figure S4 in the Supporting Information. As a result, the average length at high NaCl concentration tended to be shorter than at low NaCl concentrations. These data are supported well by Figure 3 where EPM gradually decreases as NaCl concentration increases, and reaches nearly zero when NaCl concentration was more than 10 mM.

dx.doi.org/10.1021/jp4035166 | J. Phys. Chem. B XXXX, XXX, XXX−XXX

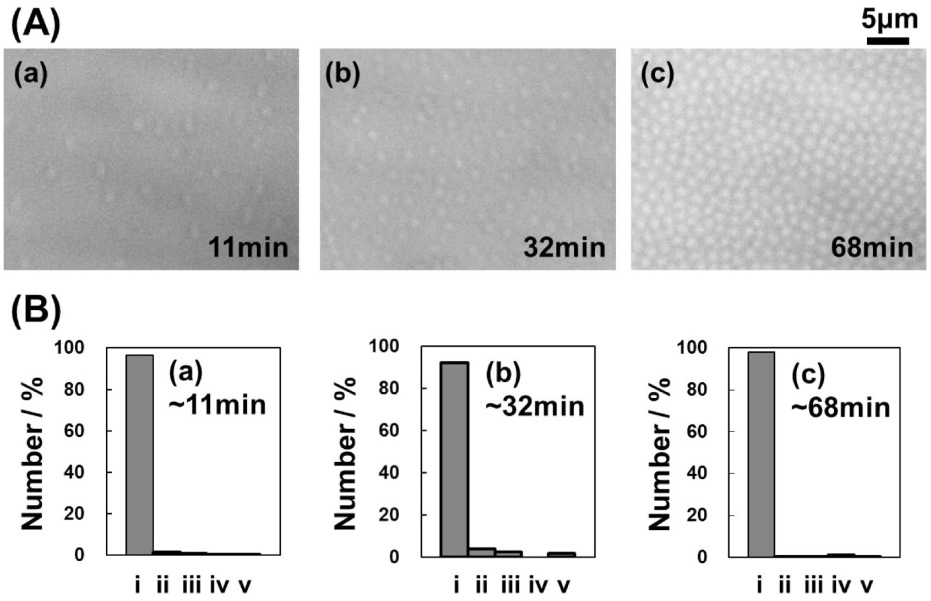

Figure 9. (A) Optical microscope observation of the binary mixtures of N(+) and N(−) microgels at 25 °C as a function of time. The images were taken (a) 11, (b) 32, and (c) 68 min after the mixing. NaCl concentration was 10 mM. Total microgel concentration was 0.0025 wt % in each case. The air/water interfaces were observed in all cases. Concentration ratio of N(+) and N(−) microgels was 1:1 (wt %/wt %). (B) Number distribution of microgels and microgel assemblies for the binary mixtures of N(+) and N(−) microgels shown in (A): (i) monomer, (ii) dimer, (iii) trimer, (iv) chainlike assembly (more than four microgels), and (v) aggregates. Microgels or microgel assemblies observed per unit area (3640 μm^2) were counted.

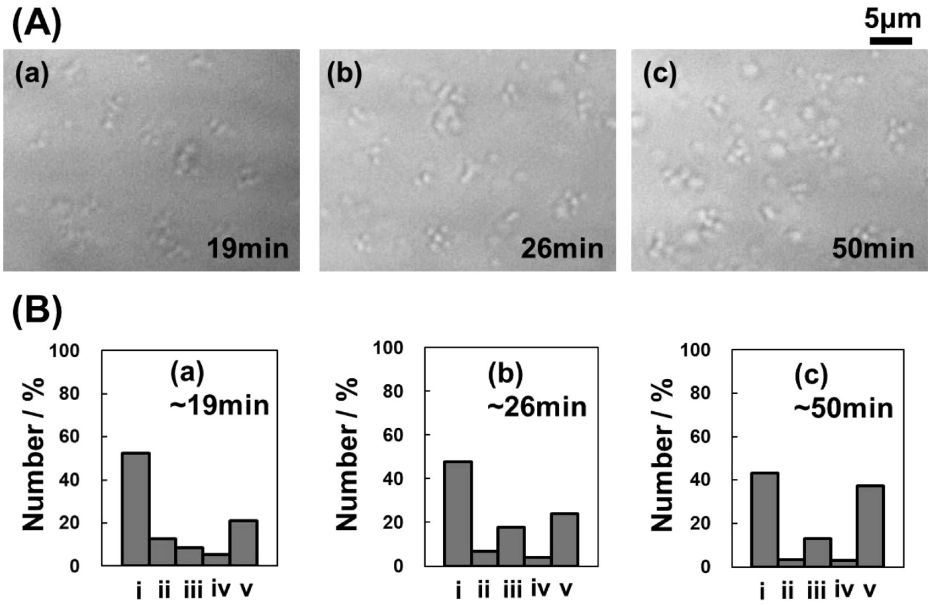

Figure 10. (A) Optical microscope observation of the binary mixtures of N(+) and N(−) microgels at 25 °C as a function of time. The images were taken (a) 19, (b) 26, and (c) 50 min after the mixing. No NaCl was added. The concentration ratio of N(+) and N(−) microgels was 1:9 (wt %/wt %). Total microgel concentration was 0.0025 wt % in each case. The air/water interfaces were observed in all cases. (B) Number distribution of microgels and microgel assemblies for the binary mixtures of N(+) and N(−) microgels shown in (A): (i) monomer, (ii) dimer, (iii) trimer, (iv) chainlike assembly (more than four microgels), and (v) aggregates. Microgels or microgel assemblies observed per unit area (3640 μm^2) were counted.

In order to clarify the mechanism of the microgel assembly at the air/water interface, the binary mixtures were observed as a function of time. Figure 6A shows representative images of microgels and microgel assemblies at the air/water interface when no NaCl is added. After 13 min, there were many single microgels and the number of microgel assemblies was small (Figure 6B(a)). As time advanced, number of microgel assemblies became larger after 27 min (Figure 6A,B(b)); however, the major assemblies were not chainlike assemblies (i.e., more than four microgels). Finally, many chainlike assemblies were formed after 49 min (Figure 6A,B(c)). Note that the number of the chainlike structure was larger than that of the other assemblies such as a dimer, trimer, and aggregate (compare Figure 6B(b) with Figure 6B(c)). The sizes of the aggregate were increased with time as shown in Table S1 (Supporting Information). The aspect ratio of the aggregate

dx.doi.org/10.1021/jp4035166 | J. Phys. Chem. B XXXX, XXX, XXX−XXX

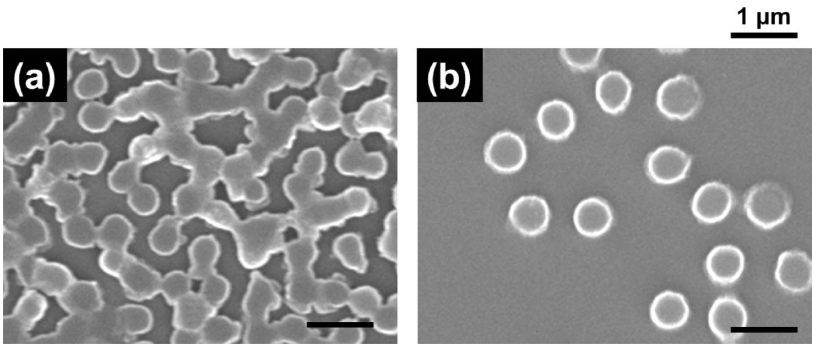

Figure 11. SEM observation of the binary mixtures of N(+) and NAD(−) microgels dried on polystyrene substrate at 25 °C. NaCl concentration was 3 mM. (a) Before and (b) after degradation of NAD(−) microgels by dropping a 5 wt % $NaIO_4$ solution on the dried structure. NaCl and $NaIO_4$ were washed with deionized water gently and repeatedly. Scale bars are 1 μm.

was 0.51: the ratio was estimated by x/y, x is the narrow side and y is the long side. The mechanism of the microgel chain formation is shown in Figure 7. At first, many N(+) and N(−) microgels are adsorbed at the air/water interface, respectively (Figure 7A). Before the adsorption of these microgels, assembly of these microgels may be suppressed compared to the sample as shown in Figure 4a where aggregation of these microgels was observed with naked eyes under the same salt concentration. This difference may be due to the difference in microgel concentration (0.05 wt % for Figure 4 and 0.0025 wt % for Figure 6), and the amount of dispersion (3 mL for Figure 4 and 20 μL for Figure 6): the air/water interface per microgels for the sample shown in Figure 6 is much larger than that shown in Figure 4. Indeed, sedimentation of microgels on the substrate was not observed for the sample shown in Figure 6 (see Figure S3(C) in the Supporting Information). After the adsorption of microgels at the air/water interface (Figure 7A), N(+) and N(−) microgels are assembled with each other near the interface (Figure 7B). As time advances, these assemblies and the microgels are attached, and the length of the chain became longer (Figure 7C, movies in the Supporting Information). Note that the lateral Brownian motion of the microgels was observed at the air/water interface, but vertical Brownian motion was not observed (SI movie files). Therefore, these microgels and their aggregates were adsorbed at the air/water interface. Finally, the microgel assemblies are formed with each other, and grow into linear and branched chains probably due to anisotropic interaction of microgel assemblies such as Janus particles (Figure 7D,E).[16,17,61]

To check NaCl dependence, the binary mixtures were observed at the air/water interface as a function of time. Figure 8A shows representative images of microgels and microgel assemblies at the air/water interfaces when NaCl concentration is 0.3 mM. The mechanism of the chain growth is similar to the sample shown in Figures 6 and 7. However, at the last stage (Figure 8A(c)), number ratio of microgel assemblies is much smaller than the sample shown in Figure 6, and there are many sole microgels (compare Figure 6B(c) with Figure 8B(c)). Taking the data shown in Figure 4d where microgels show slow flocculation under the same salt concentration into consideration, the data shown in Figure 8 suggests that microgel flocculation seems to be suppressed at the air/water interface. With increasing NaCl concentration, microgels were not assembled with each other at the air/water interface (Figure 9), and the number of the monomers was 82, 281, and 1117 at (a) 11 min, (b) 32 min, (c) 68 min, respectively. In this case, the number was almost equal after 68 min. Then, the hexagonally ordered structures were formed as has been previously reported by using sole pNIPAm microgels.[60]

Furthermore, the influence of concentration ratio of N(+) and N(−) microgels on the microgel assembly was investigated. Figure 10A shows representative images of microgels and microgel assemblies at the air/water interface when no NaCl is added. Herein, the concentration ratio of N(+) and N(−) microgels was 1:9 (wt %/wt %). Different from the results in the case of the concentration ratio 1:1 (wt %/wt %) (Figure 6), the number of random aggregation was increased (Figure 10B(v)), indicating that the concentration ratio of N(+) and N(−) microgels is an important factor to form microgel chains. Here, the average size of the aggregates was ∼4 μm, and the aspect ratio was 0.75 at 50 min (Table S1). By comparing the aggregates shown in Figures 6 and 10, where the aggregates were formed without and with NaCl, respectively, the size and shape of the aggregates were different. The structure of the aggregates shown in Figure 10 may be as follows: a cationic microgel was surrounded by several anionic microgels, thus the raspberry-like aggregates prevented them from further aggregation, although the shape of the aggregates was not uniform.

To clarify the structure of the microgel chains, anionic and degradable microgels, NAD(−), were used for the investigation. In this case, N(+) and NAD(−) microgel dispersions were mixed; the microgel concentrations were 0.0025 wt %, and NaCl concentrations were 3 mM for both dispersions. They also formed microgel chains at the air/water interface similar to the results shown in Figure 6. The dispersion was dried on the polystyrene substrate, then the substrate was observed by SEM after washing NaCl with water. Figure 11a reveals that these microgels are indeed connected to each other, which is different from conventional pNIPAm thin films.[18,60] Here, the fractal dimension of the aggregates (Figure 11a) was estimated by the following relationship and box-counting analysis[62,63]

$$N(r) \propto r^{-Df}$$

where $N(r)$ is the number of the boxes (grids) containing different fracture features and r is the box size. As a result, the dimension was 1.88 (Figure S5 in the Supporting Information).[64] After degrading NAD(−) microgels by dropping a 5 wt % $NaIO_4$ solution on the overall dried structure, the microgel network structure was not observed, and the microgels were not connected each other (Figure 11b). These data also support this study that microgel chains were formed due to electrostatic attractive force between cationic and anionic

dx.doi.org/10.1021/jp4035166 | J. Phys. Chem. B XXXX, XXX, XXX−XXX

microgels as shown in Figure 7. Further investigations are in progress to create more precisely controlled one-dimensional microgel structures by using anisotropic microgels.

CONCLUSION

Monodispersed and oppositely charged microgels were synthesized by aqueous free-radical precipitation polymerization of NIPMAm and cross-linkers by using different types of water-soluble initiators and comonomers. These microgels were large enough to be traced by optical microscopy. EPM of these microgels could be changed by addition of a small amount of NaCl, and EPM values were almost zero when more than 10 mM NaCl was added. By using these microgels, linear and branched-chain structures of microgels could be obtained near the air/water interface. Because of the adsorption of microgels at the air/water interface, the rate of microgel assembly became slower than inside of a solution. In addition, we found that total microgel concentration, concentration ratio of cationic and anionic microgels, and salt concentration were important factors to create the microgel chains. Our new findings to form the microgel chains by simply mixing oppositely charged microgels will lead to creation of more complex one-dimensional structures such as double-helix structure of particles by controlling the geometry of the particle itself.

ASSOCIATED CONTENT

Supporting Information

Phase diagram of binary mixtures of N(+) and N(−) microgels as a function of temperature and salt concentration, optical microscope images of the binary mixtures at 25 °C as a function of time and total microgel concentration, the length of the linear and branched chainlike structures at different salt concentrations, the fractal dimension of the aggregates of N(+) and NAD(−) microgels, the aggregation behavior of the microgels at the air/water interface, and the size of the aggregates at each time. This material is available free of charge via the Internet at http://pubs.acs.org.

AUTHOR INFORMATION

Corresponding Author

*E-mail: d_suzuki@shinshu-u.ac.jp.

Notes

The authors declare no competing financial interest.

ACKNOWLEDGMENTS

D.S. acknowledges Grant-in-Aid for Challenging Exploratory Research from the Ministry of Education, Culture, Sports, Science, and Technology of Japan (24655206). This work was partially supported by the program for Dissemination of Tenure-Track System funded by the Ministry of Education and Science, Japan. The authors thank Yoshitaka Umeda for his help in preparing NAD(−) microgels.

REFERENCES

(1) Sun, S.; Murray, C. B.; Weller, D.; Folks, L.; Moser, A. Monodisperse FePt Nanoparticles and Ferromagnetic FePt Nanocrystal Superlattices. *Science* **2000**, *287*, 1989−1992.

(2) Ozbay, E. Plasmonics: Merging Photonics and Electronics at Nanoscale Dimensions. *Science* **2006**, *311*, 189−193.

(3) Grzelczak, M.; Vermant, J.; Furst, E. M.; Liz-Marzán, L. M. Directed Self-Assembly of Nanoparticles. *ACS Nano* **2010**, *4*, 3591−3605.

(4) Tang, Z.; Kotov, N. A. One-Dimentional Assemlies of Nanoparticles: Preparation, Properties, and Promise. *Adv. Mater.* **2005**, *17*, 951−962.

(5) Wang, H.; Patil, A. J.; Liu, K.; Petrov, S.; Mann, S.; Winnik, M. A.; Manners, I. Fabrication of Continuous and Segmented Polymer/Metal Oxide Nanowires Using Cylindrical Micelles and Block Comicelles as Templates. *Adv. Mater.* **2009**, *21*, 1805−1808.

(6) Ostrov, N.; Gazit, E. Genetic Engineering of Biomolecular Scaffolds for the Fabrication of Organic and Metallic Nanowires. *Angew. Chem., Int. Ed.* **2010**, *49*, 3018−3021.

(7) Masuda, H.; Fukuda, K. Ordered Metal Nanohole Arrays Made by a Two-step Replication of Honeycomb Structures of Anodic Alumina. *Science* **1995**, *268*, 1466−1468.

(8) Correa-Duarte, M. A.; Liz-Marzán, L. M. Carbon Nanotubes as Templates for One-Dimentional Nanoparticle Assemblies. *J. Mater. Chem.* **2006**, *16*, 22−25.

(9) Lu, Y.; Yin, Y.; Li, Z. Y.; Xia, Y. Synthesis and Self-Assembly of Au@SiO_2 Core-Shell Colloids. *Nano Lett.* **2002**, *2*, 785−788.

(10) Hu, Y.; He, L.; Yin, Y. Magnetically Responsive Photonic Nanochains. *Angew. Chem., Int. Ed.* **2011**, *50*, 3747−3750.

(11) Li, M.; Johnson, S.; Guo, H.; Dujardin, E.; Mann, S. A Generalized Mechanism for Ligand-Induced Dipolar Assembly of Plasmonic Gold Nanoparticle Chain Networks. *Adv. Funct. Mater.* **2011**, *21*, 851−859.

(12) Ma, M.; Zhang, Q.; Dou, J.; Zhang, H.; Geng, W.; Yin, D.; Chen, S. Fabrication of 1D Fe_3O_4/P(NIPAM-MBA) Thermosensitive Nanochains by Magnetic-Field-Induced Precipitation Polymerization. *Colloid Polym. Sci.* **2012**, *290*, 1207−1213.

(13) Zhang, L.; Zhu, Y. Directed Assembly of Janus Particles under High Frequency ac- Electric Fields: Effects of Medium Conductivity and Colloidal Surface Chemistry. *Langmuir* **2012**, *28*, 13201−13207.

(14) Cayre, O.; Paunov, V. N.; Velev, O. D. Fabrication of Asymmetrically Coated Colloid Particles by Microcontact Printing Techniques. *J. Mater. Chem.* **2003**, *13*, 2445−2450.

(15) Suzuki, D.; Tsuji, S.; Kawaguchi, H. Development of Anisotoropic Thermo-Sensitive Hairy Particles Using Living Radical Graft Polymerization. *Chem. Lett.* **2005**, *34*, 242−243.

(16) Suzuki, D.; Tsuji, S.; Kawaguchi, H. Janus Microgels Prepared by Surfactant-Free Pickering Emulsion-Based Modification and Their Self-Assembly. *J. Am. Chem. Soc.* **2007**, *129*, 8088−8089.

(17) Umeda, Y.; Kobayashi, T.; Hirai, T.; Suzuki, D. Effects of pH and Temperature on Assembly of Multiresponsive Janus Microgels. *Colloid Polym. Sci.* **2011**, *289*, 729−737.

(18) Pelton, R. H.; Chibante, P. Preparation of Aqueous Latices with *N*-Isopropylacrylamide. *Colloids Surf.* **1986**, *20*, 247−256.

(19) Saunders, B. R.; Vincent, B. Microgel Particles as Model Colloids: Theory, Properties and Applications. *Adv. Colloid Interface Sci.* **1999**, *80*, 1−25.

(20) Hayashi, H.; Iijima, M.; Kataoka, K.; Nagasaki, Y. pH-Sensitive Nanogel Possessing Reactive PEG Tethered Chains on the Surface. *Macromolecules* **2004**, *37*, 5389−5396.

(21) Hoare, T.; Pelton, R. Functional Group Distributions in Carboxylic Acid Containing Poly(*N*-isopropylacrylamide) Microgels. *Langmuir* **2004**, *20*, 2123−2133.

(22) Hoare, T.; Pelton, R. Characterizing Charge and Crosslinker Distributions in Polyelectrolyte Microgels. *Curr. Opin. Colloid Interface Sci.* **2008**, *13*, 413−428.

(23) Sershen, S. R.; Westcott, S. L.; Halas, N. J.; West, J. L. Temperature-Sensitive Polymer−Nanoshell Composites for Photothermally Modulated Drug Delivery. *J. Biomed. Mater. Res.* **2000**, *51*, 293−298.

(24) Nayak, S.; Lyon, L. A. Photoinduced Phase Transitions in Poly(*N*-isopropylacrylamide) Microgels. *Chem. Mater.* **2004**, *16*, 2623−2627.

(25) Suzuki, D.; Sakai, T.; Yoshida, R. Self-Flocculating/Self-Dispersing Oscillation of Microgels. *Angew. Chem., Int. Ed.* **2008**, *47*, 917−920.

(26) Suzuki, D.; Taniguchi, H.; Yoshida, R. Autonomously Oscillating Viscosity in Microgel Dispersions. *J. Am. Chem. Soc.* **2009**, *131*, 12058−12059.
(27) Hsiue, G. H.; Hsu, S. H.; Yang, C. C.; Lee, S. H.; Yang, I. K. Preparation of Controlled Release Ophthalmic Drops, for Glaucoma Therapy Using Thermosensitive Poly-*N*-isopropylacrylamide. *Biomaterials* **2002**, *23*, 457−462.
(28) Nayak, S.; Lee, H.; Chmielewski, J.; Lyon, L. A. Folate-Mediated Cell Targeting and Cytotoxicity Using Thermoresponsive Microgels. *J. Am. Chem. Soc.* **2004**, *126*, 10258−10259.
(29) Tamura, A.; Oishi, M.; Nagasaki, Y. Enhanced Cytoplasmic Delivery of siRNA Using a Stabilized Polyion Complex Based on PEGylated Nanogels with a Cross-Linked Polyamine Structure. *Biomacromolecules* **2009**, *10*, 1818−1827.
(30) Morris, G. E.; Vincent, B.; Snowden, M. J. Adsorption of Lead Ions onto *N*-Isopropylacrylamide and Acrylic Acid Copolymer Microgels. *J. Colloid Interface Sci.* **1997**, *190*, 198−205.
(31) Kawaguchi, H.; Kisara, K.; Takahashi, T.; Achiha, K.; Yasui, M.; Fujimoto, K. Versatility of Thermosensitive Particles. *Macromol. Symp.* **2000**, *151*, 591−598.
(32) Weissman, J. M.; Sunkara, H. B.; Tse, A. S.; Asher, S. A. Thermally Switchable Periodicities and Diffraction from Mesoscopically Ordered Materials. *Science* **1996**, *274*, 959−960.
(33) Lyon, L. A.; Debord, J. D.; Debord, S. B.; Jones, C. D.; McGrath, J. G.; Serpe, M. J. Microgel Colloidal Crystals. *J. Phys. Chem. B* **2004**, *108*, 19099−19108.
(34) Suzuki, D.; McGrath, J. G.; Kawaguchi, H.; Lyon, L. A. Colloidal Crystals of Thermosensitive, Core/Shell Hybrid Microgels. *J. Phys. Chem. C* **2007**, *111*, 5667−5672.
(35) Okubo, T.; Suzuki, D.; Yamagata, T.; Katsuno, A.; Sakurai, M.; Kimura, H.; Tsuchida, A. Colloidal Crystallization of Thermo-Sensitive Gel Spheres of Poly (*N*-isopropyl acrylamide). *Colloid Polym. Sci.* **2011**, *289*, 291−299.
(36) Fujii, S.; Read, E. S.; Binks, B. P.; Armes, S. P. Stimulus-Responsive Emulsifiers Based on Nanocomposite Microgel Particles. *Adv. Mater.* **2005**, *17*, 1014−1018.
(37) Brugger, B.; Richtering, W. Emulsions Stabilized by Stimuli-Sensitive Poly(*N*-isopropylacrylamide)-*co*-Methacrylic Acid Polymers: Microgels versus Low Molecular Weight Polymers. *Langmuir* **2008**, *24*, 7769−7777.
(38) Suzuki, D.; Yamakawa, S. Hydrogel Particles as a Particulate Stabilizer for Dispersion Polymerization. *Langmuir* **2012**, *28*, 10629−10634.
(39) Zhang, J.; Xu, S.; Kumacheva, E. Polymer Microgels: Reactors for Semiconductor, Metal, and Magnetic Nanoparticles. *J. Am. Chem. Soc.* **2004**, *126*, 7908−7914.
(40) Pich, A.; Hain, J.; Lu, Y.; Boyko, V.; Prots, Y.; Adler, H. J. Hybrid Microgels with ZnS Inclusions. *Macromolecules* **2005**, *38*, 6610−6619.
(41) Lu, Y.; Mei, Y.; Ballauff, M.; Drechsler, M. Thermosensitive Core-Shell Particles as Carrier Systems for Metallic Nanoparticles. *J. Phys. Chem. B* **2006**, *110*, 3930−3937.
(42) Suzuki, D.; Kawaguchi, H. Modification of Gold Nanoparticle Composite Nanostructures Using Thermosensitive Core-Shell Particles as a Template. *Langmuir* **2005**, *21*, 8175−8179.
(43) Suzuki, D.; Kawaguchi, H. Stimuli-Sensitive Core/Shell Template Particles for Immobilizing Inorganic Nanoparticles in the Core. *Colloid Polym. Sci.* **2006**, *284*, 1443−1451.
(44) Serpe, M. J.; Kim, J.; Lyon, L. A. Colloidal Hydrogel Microlenses. *Adv. Mater.* **2004**, *16*, 184−187.
(45) Kim, J.; Serpe, M. J.; Lyon, L. A. Photoswitchable Microlens Arrays. *Angew. Chem., Int. Ed.* **2005**, *44*, 1333−1336.
(46) Sorrell, C. D.; Carter, M. C. D.; Serpe, M. J. Color Tunable Poly(*N* -Isopropylacrylamide)- *co* -Acrylic Acid Microgel−Au Hybrid Assemblies. *Adv. Funct. Mater.* **2011**, *21*, 425−433.
(47) Sorrell, C. D.; Lyon, L. A. Deformation Controlled Assembly of Binary Microgel Thin Films. *Langmuir* **2008**, *24*, 7216−7222.
(48) Meng, Z.; Smith, M. H.; Lyon, L. A. Temperature-Programmed Synthesis of Micron-Sized Multi-Responsive Microgels. *Colloid Polym. Sci.* **2009**, *287*, 277−285.
(49) Guillermo, A.; Cohen Addad, J. P.; Bazile, J. P.; Duracher, D.; Elaissari, A.; Pichot, C. NMR Investigations into Heterogeneous Structures of Thermosensitive Microgel Particles. *J. Polym. Sci., Part B: Polym. Phys.* **2000**, *38*, 889−898.
(50) Berndt, I.; Richtering, W. Doubly Temperature Sensitive Core-Shell Microgels. *Macromolecules* **2003**, *36*, 8780−8785.
(51) Daly, E.; Saunders, B. R. Temperature-Dependent Electrophoretic Mobility and Hydrodynamic Radius Measurements of Poly(*N*-isopropylacrylamide) Microgel Particles: Structural Insights. *Phys. Chem. Chem. Phys.* **2000**, *2*, 3187−3193.
(52) Suzuki, D.; Horigome, K. Binary Mixtures of Cationic and Anionic Microgels. *Langmuir* **2011**, *27*, 12368−12374.
(53) Spruijt, E.; Bakker, H. E.; Kodger, T. E.; Sprakel, J.; Stuart, M. A. C.; van der Gucht, J. Reversible Assembly of Oppositely Charged Hairy Colloids in Water. *Soft Matter* **2011**, *7*, 8281−8290.
(54) Russell, E. R.; Sprakel, J.; Kodger, T. E.; Weitz, D. A. Colloidal Gelation of Oppositely Charged Particles. *Soft Matter* **2012**, *8*, 8697−8703.
(55) Vincent, B. The van der Waals Attraction Between Colloid Particles Having Adsorbed Layers. II. Calculation of Interaction Curves. *J. Colloid Interface Sci.* **1973**, *42*, 270−285.
(56) Heskins, M.; Guillet, J. E. Solution Properties of Poly(*N*-isopropylacrylamide). *J. Macromol. Sci., Chem.* **1968**, *A2*, 1441−1455.
(57) Schild, H. G. Poly(N-isopropylacrylamide): Experiment, Theory and application. *Prog. Polym. Sci.* **1992**, *17*, 163−249.
(58) Zhang, J.; Pelton, R. Poly(*N*-isopropylacrylamide) at the Air/Water Interface. *Langmuir* **1996**, *12*, 2611−2612.
(59) Zhang, J.; Pelton, R. Poly(*N*-isopropylacrylamide) Microgels at the Air-Water Interface. *Langmuir* **1999**, *15*, 8032−8036.
(60) Horigome, K.; Suzuki, D. Drying Mechanism of Poly(N-isopropylacrylamide) Microgel Dispersions. *Langmuir* **2012**, *28*, 12962−12970.
(61) Hong, L.; Cacciuto, A.; Luijten, E.; Granick, S. Clusters of Charged Janus Spheres. *Nano Lett.* **2006**, *6*, 2510−2514.
(62) Sahimi, M. Flow Phenomena in Rocks: from Continuum Models to Fractals, Percolation, Cellular Automata, and Simulated Annealing. *Rev. Mod. Phys.* **1993**, *65*, 1393−1534.
(63) Kanniah, V.; Wu, P.; Mandzy, N.; Grulke, E. A. Fractal Analysis as a Complimentary Technique for Characterizing Nanoparticle Size Distributions. *Powder Technol.* **2012**, *226*, 189−198.
(64) Rasmusson, M.; Routh, A.; Vincent, B. Flocculation of Microgel Particles with Sodium Chloride and Sodium Polystyrene Sulfonate as a Function of Temperature. *Langmuir* **2004**, *20*, 3536−3542.